ISTITUTO NAZIONALE DI FISICA NUCLEARE

Sezione di Lecce

INFN/TC-98/06
26 Febbraio 1998

TEST OF A SILICA AEROGEL THRESHOLD CHERENKOV COUNTER FOR THE TJNAF HALL A SPECTROMETERS WITH 1-4 GeV/c PARTICLES

R. Perrino, L. Lagamba, E. Cisbani, S. Colilli, R. Crateri, R. De Leo, S. Frullani, F. Garibaldi, F. Giuliani, M. Gricia, M. Iodice, A. Leone, M. Lucentini, A. Mostarda, E. Nappi, L. Pierangeli, F. Santavenere, G.M. Urciuoli

PACS number(s): 29.40.Mc

SIS–Pubblicazioni
dei Laboratori Nazionali di Frascati

INFN - Istituto Nazionale di Fisica Nucleare
Sezione di Lecce

INFN/TC–98/06
26 Febbraio 1998

TEST OF A SILICA AEROGEL THRESHOLD CHERENKOV COUNTER FOR THE TJNAF HALL A SPECTROMETERS WITH 1-4 GeV/c PARTICLES

R. Perrino[a], L. Lagamba[b], E. Cisbani[c], S. Colilli[c], R. Crateri[c], R. De Leo[b], S. Frullani[c], F. Garibaldi[c], F. Giuliani[c], M. Gricia[c], M. Iodice[c], A. Leone[a], M. Lucentini[c], A. Mostarda[c], E. Nappi[b], L. Pierangeli[c], F. Santavenere[c], G.M. Urciuoli[c]

[a]INFN - Sezione di Lecce, via per Arnesano, I–73100 Lecce, Italy
[b]Dipartimento Interateneo di Fisica and INFN - Sezione di Bari
via Amendola 173, I–70126 Bari, Italy
[c]Laboratorio di Fisica dell'Istituto Superiore di Sanita' and INFN - Sezione Sanita'
viale Regina Elena 299, I–00161 Roma, Italy

Abstract

The silica aerogel threshold Cherenkov counter for the Jefferson Lab Hall A spectrometers has been tested at CERN with a beam of positrons, pions and protons in order to characterize its efficiencies to particle detection in the 1 to 4 GeV/c momentum range. A detection efficiency to particles above the Cherenkov threshold (e^+ and π^+) greater than 95% and to particles below the threshold (p) of about 5% has been quoted in the whole momentum range explored. The detection efficiency to protons is due both to induced δ-rays production (3.5%), and to accidentals due to the high counting rate.

INFN - Istituto Nazionale di Fisica Nucleare
Sezione di Lecce

INFN/TC–98/06
26 Febbraio 1998

TEST OF A SILICA AEROGEL THRESHOLD CHERENKOV COUNTER FOR THE TJNAF HALL A SPECTROMETERS WITH 1-4 GeV/c PARTICLES

R. Perrino[a], L. Lagamba[b], E. Cisbani[c], S. Colilli[c], R. Crateri[c], R. De Leo[b], S. Frullani[c], F. Garibaldi[c], F. Giuliani[c], M. Gricia[c], M. Iodice[c], A. Leone[a], M. Lucentini[c], A. Mostarda[c], E. Nappi[b], L. Pierangeli[c], F. Santavenere[c], G.M. Urciuoli[c]

[a]INFN - Sezione di Lecce, via per Arnesano, 73100 Lecce, Italy
[b]Dipartimento Interateneo di Fisica and INFN - Sezione di Bari
via Amendola 173, I–70126 Bari, Italy
[c]Laboratorio di Fisica dell'Istituto Superiore di Sanita' and INFN - Sezione Sanita'
viale Regina Elena 299, I–00161 Roma, Italy

Abstract

The silica aerogel threshold Cherenkov counter for the Jefferson Lab Hall A spectrometers has been tested at CERN with a beam of positrons, pions and protons in order to characterize its efficiencies to particle detection in the 1 to 4 GeV/c momentum range. A detection efficiency to particles above the Cherenkov threshold (e^+ and π^+) greater than 95% and to particles below the threshold (p) of about 5% has been quoted in the whole momentum range explored. The detection efficiency to protons is due both to induced δ-rays production (3.5%), and to accidentals due to the high counting rate.

1 Introduction

In Hall A at the Thomas Jefferson National Accelerator Facility (TJNAF, formerly known as CEBAF) the nucleus structure will be investigated through the measurement of hadron knock-out reactions induced by an electron beam of energy up to 6 GeV. This experimental area is equipped with two high resolution magnetic spectrometers (HRS) for coincidence measurements by detecting both the scattered electron and the knocked out hadron, respectively [1]. The spectrometers are designed to achieve a momentum resolution better than 10^{-4} and are equipped with a set of detectors for trigger definition, momentum measurement and a full identification of charged particles. In particular, a good separation capability is required for electron and pion in the electron arm, and for pion and proton in the hadron arm spectrometer up to momenta of 4 GeV/c. To this aim, two different threshold Cherenkov counters have been developed by a collaboration among INFN-Sanita', INFN-Lecce, INFN-Bari, the University of Regina (Canada) and the CEN–Saclay (France). In the first detector, a 1 m thick volume of CO_2 is used as radiator [2]. The second one uses 9 cm thick silica aerogel with index of refraction $n = 1.025$ [3,4]. A set of such detectors are currently being installed at TJNAF in each of the two Hall A spectrometers.

In the present work we report on the absolute detection efficiency of the aerogel device to particles (e^+,π^+) well above the Cherenkov threshold, and on the rejection ratio to sub-threshold particles (p). To this purpose, we have exposed the detector to a multiparticle beam with momenta between 1 and 4 GeV/c. Previous tests on the same detector were done [4] with only one type of particles (e^-). General information about the detector, the silica aerogel properties and the photodetectors used, are given in *Sect.* 2. The experimental method and the discussion of the results are illustrated in the following *Sect.* 3. In *Sect.* 4 we draw some summarizing conclusions.

2 Detector configuration, silica aerogel properties and phototubes calibration

2.1 The detector

The details of the aerogel Cherenkov counter, subject of the present work, have already been discussed in Refs. [3,4], therefore here we only report a brief description. The counter is made of 13 sections, each equipped with two 14-stage, head-on, 5" BURLE 8854 Quantacon photomultiplier tubes (PMT) [5]. These PMTs have high quantum efficiency (quoted 22.5% at maximum

response wavelength), good spectral response matching with the ultraviolet radiation transmitted by the aerogel, fast signals and high current gain. The aerogel tiles, each 3 *cm* thick, are arranged in the detector tray, to form a total radiator thickness $L = 9$ *cm*. Since a (π, p) discrimination is required to this detector in the 1 to 4 GeV/c range, the chosen aerogel index of refraction is $n = 1.025$, that corresponds to Cherenkov thresholds of 0.62 GeV/c and 4.2 GeV/c for pions and for protons, respectively. A cross–sectional drawing of the detector is shown in Fig. 1, where the aerogel tiles location and the mirror profile are sketched. In Fig. 2, the detector front view is shown.

2.2 Silica aerogel properties

Silica aerogel is as well matched as a radiator for threshold Cherenkov counters that operate at low–intermediate momentum ranges, which are typical of TJNAF. The available aerogel with index of refraction from 1.005 to 1.13 is the best alternative to pressurized gas. The Cherenkov counter here discussed uses aerogel tiles with index of refraction $n = 1.025$, provided by Airglass [6].

The main drawback of aerogel is a poor optical transmission: a fraction of Cherenkov photons produced in the aerogel is absorbed and a more consistent fraction is Rayleigh scattered. The light directly transmitted through an aerogel block of thickness d, as a function of the wavelength λ, is proportional to e^{-Cd/λ^4}, where the constant C characterizes the clarity of the aerogel. The transmission curve for the Airglass aerogel used in the present work, measured with a photospectrometer, is plotted in Fig. 3. The experimental points are well represented by the equation $T = A \exp(-Cd/\lambda^4)$, where the parameter A accounts for the absorption at high wavelengths.

The parameters C and A for the aerogel used in this work, evaluated by fitting the experimental points in Fig. 3, result to be $C = (0.021 \pm 0.006)\ \mu m^4/cm$ and $A = (0.96 \pm 0.08)$. The obtained value of C indicates a rather modest clarity of the aerogel samples used, when compared to other aerogels (data reported in Tab. 1), from the same manufacturer [7] and from the KEK Laboratory in Japan [8].

2.3 Calibration of the phototube responses

The correct operation of the Cherenkov counter needs a characterization of the phototube response in order to get the single photoelectron resolution and the average number of photoelectrons detected, μ. In addition, for an evaluation of the phototube gain, the one photoelectron (*p.e.*) peak (OPP) position is the relevant parameter to be measured.

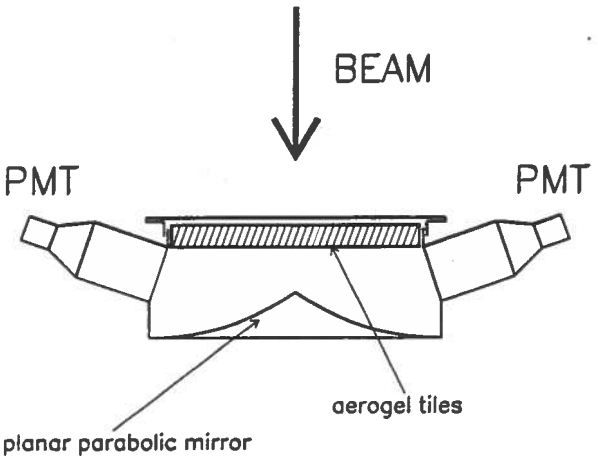

Fig. 1. Cross–sectional view of the aerogel counter showing the radiator thickness and mirror profile.

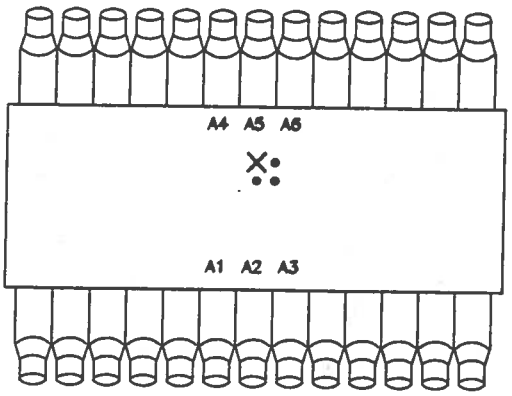

Fig. 2. Schematic drawing of the aerogel counter as viewed by the incoming beam during the test. The photomultipliers used in this work are conventionally labeled from $A1$ to $A6$, as reported in the text. The cross marks the beam impact point chosen for the detailed discussion of results. Dots show the beam impact points in which the detector response has been studied versus impact position.

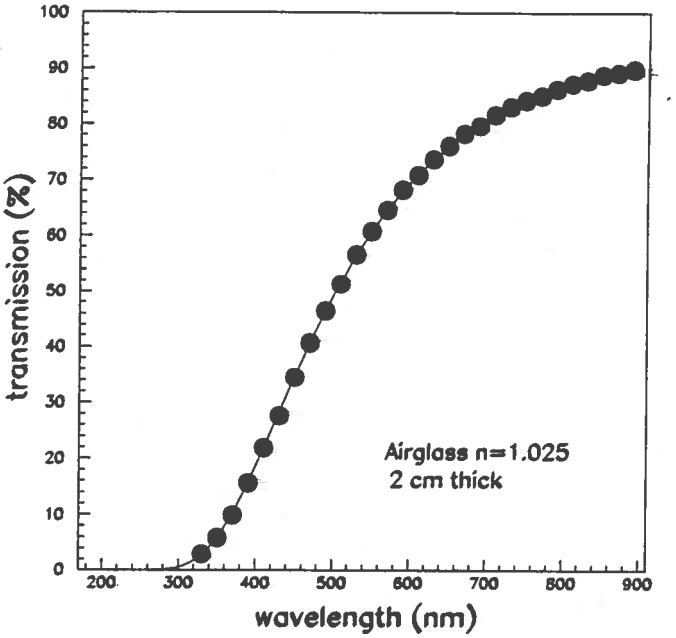

Fig. 3. Light transmission as a function of wavelength measured with a spectrophotometer for the aerogel used in this work. The sample thickness is $d = 2\ cm$. The curve is obtained by fitting the data with the formula $T = A \exp(-Cd/\lambda^4)$, where $A = (0.96 \pm 0.08)$ and $C = (0.021 \pm 0.006)\ \mu m^4/cm$.

Table 1
Results of measurements of transmission for the aerogel used in the present work, compared to different types of aerogel of same thickness.

Aerogel sample	C $(\mu m^4/cm)$	A	*Transmission* @350 *nm* (%)	Ref.
Airglass $n = 1.025$	0.021 ± 0.006	0.96 ± 0.08	3×10^{-6}	*This work*
Airglass $n = 1.030$	0.0183	0.96	3×10^{-5}	[7]
KEK $n = 1.018$	0.0097 ± 0.0002	0.96 ± 0.01	3×10^{-3}	[8]
KEK $n = 1.029$	0.0114 ± 0.0002	0.96 ± 0.01	1×10^{-3}	[8]

The calibration measurements of every detector phototube were performed using the Berkeley Nucleonics Corporation Mod. 6010 Light Pulse Generator as a photon source. The light source repetition rate was set to 1 kHz, with a pulse duration of 20 ns. The intensity was instead adjusted with the aim to increase the number of *p.e.*s emitted by the photocathode. The phototube output signal, discriminated through a leading edge discriminator, was used in coincidence with the pulser trigger, to generate the gate for charge integration. In this way the pedestal is removed from the data, and only those events corresponding to the excitation of more than zero *p.e.*s are registered. The analog signal was charge analyzed by a LeCroy 2249W analog to digital converter (ADC). The ADC data were then acquired by a computer code onto memory storage media, and the resulting spectra were analyzed off–line. For each phototube the response spectrum was measured, for a given voltage, at different light source intensities to study the phototube response for an increasing number of *p.e.*s detected.

Examples of calibration spectra, as obtained through the procedure described above, are displayed in Fig. 4. In Fig. 4a, the case of low intensity light pulse is shown, while in Fig. 4b, the same phototube is excited by a higher intensity pulse, resulting in a more complex response spectrum made of several *p.e.*s.

The analysis of the photoexcitation spectra has been carried out by using a spectrum fitting procedure to calibrate the response scale in number of *p.e.*s rather than ADC channels. This is particularly relevant for a reliable estimate of the average number of *p.e.*s produced in a Cherenkov event.

Following Ref. [9], we have adopted a function to fit the PMT response, which is a convolution of Gaussians with a Poisson distribution. The Gaussians corresponding to the excitation of $k = 1, 2, 3, 4, ...$ *p.e.*s have been assumed to have a standard deviation given by $\sigma_k = \sqrt{k}\sigma_1$. The position of the k-th peak is given by $Q_k = Q_1 + (k-1)d$, where Q_1 is the OPP position and d is the interpeak distance.

Assuming the probability of emitting exactly k *p.e.*s is equal to:

$$P(k;\mu) = \frac{\mu^k e^{-\mu}}{k!} \tag{1}$$

the PMT response can be represented by the following function of q (expressed in ADC channels), which accounts for a normalization factor A needed for fitting the measured data:

$$f(q) = A \times \left(PED + \sum_{k=1}^{N_{max}} \frac{\mu^k e^{-\mu}}{k!} \times \frac{1}{\sigma_1 \sqrt{2\pi k}} \exp\left(-\frac{(q-Q_k)^2}{2k\sigma_1^2} \right) \right) \tag{2}$$

where $PED = 0$ when no pedestal is measured. The chosen formula thus depends upon five parameters (A,Q_1, σ_1, d, μ) to be determined by fitting

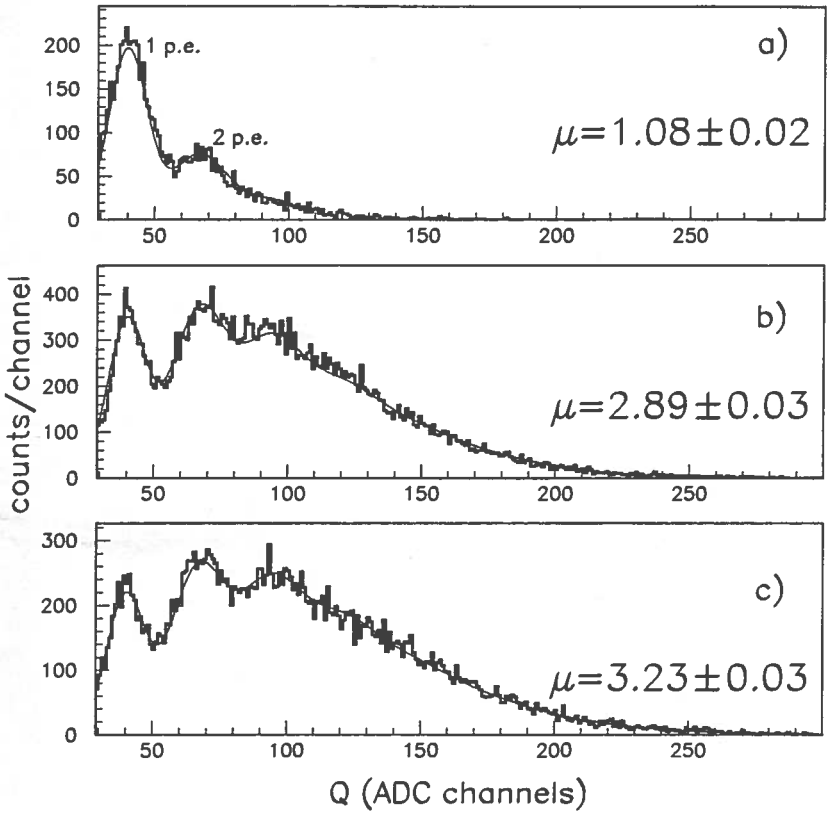

Fig. 4. Comparison of calibration spectra for one of the phototubes sampled: a) calibration measurement using low–intensity light pulses; b) calibration measurement with higher–intensity light pulses; c) response to Cherenkov light generated by the pion beam at $p = 2$ GeV/c. The 1- and 2-$p.e.$ peaks locations are indicated. The solid line that fit the spectra is the result of the peak fitting procedure as described in the text. The average numbers of $p.e.$ μ which are displayed, have been calculated with all the other parameters kept fixed.

the data. Typical results of such an analysis, carried out for the PMTs here used, are shown in Fig. 4. Here, three situations are represented: in *a)* a PMT response to low intensity light is fitted with a low average number of *p.e.*s μ, and the parameters Q_1, σ_1, d, are determined; in *b)* the same PMT response to a higher intensity light is analyzed by keeping fixed the peaks parameters, as indicated in the previous case, while the only μ is searched for. In case *c)*, the same technique is applied to the response of the PMT to Cherenkov light during the beam test, showing full consistency with the calibrated parameters.

Whenever also the pedestal is measured, it is fitted by a Gaussian peak weighted by a Poisson probability $e^{-\mu}$, including a decreasing exponential tail, which simulates the sources of background, other than the zero-*p.e.* counts, according to the formula [9]:

$$PED = e^{-\mu}\left\{\frac{1-w}{\sigma_0\sqrt{2\pi}}\exp\left(-\frac{(q-Q_0)^2}{2\sigma_0^2}\right) + w\theta(q-Q_0)\frac{1}{\lambda}e^{-\frac{q-Q_0}{\lambda}}\right\} \qquad (3)$$

where $\theta(q-Q_0) = 0$ if $q < Q_0$, $\theta(q-Q_0) = 1$ elsewhere. In this case the additional parameters Q_0, σ_0, λ, w, are introduced.

The parameters for each PMT have been derived from such an analysis, showing some little fluctuations. As far as the parameter d is concerned, we have observed that, with increasing bias voltage, the dependence of the photopeak position on the parameter d is no longer linear, showing an effect of saturation. In particular, d remains nearly constant up to about 2600 V. Since preserving the linearity of the PMT response is critical for an accurate determination of the average number of *p.e.*s, we have decided to keep the high voltage at 2500 V.

3 Results of the beam test

3.1 Experimental set-up and method

The tests here reported have been carried out at the East PS T10 test area [10] of CERN in Geneva. A beam composed of protons, pions and positrons has been used to measure the detector response at four momentum settings: $1, 2, 3$ and $4\ GeV/c$.

A schematic view of the experimental set–up is shown in Fig. 5. The beam direction was defined through the coincidence of three aligned finger counters S1, S2, S3, made of BC408 plastic scintillator. This information was used to define the hit point on the aerogel Cherenkov test counter (AC). S1 and S2, with sizes of $5 \times 5 \times 1\ cm^3$, were set $10.25\ m$ apart, S1 located just at the beam

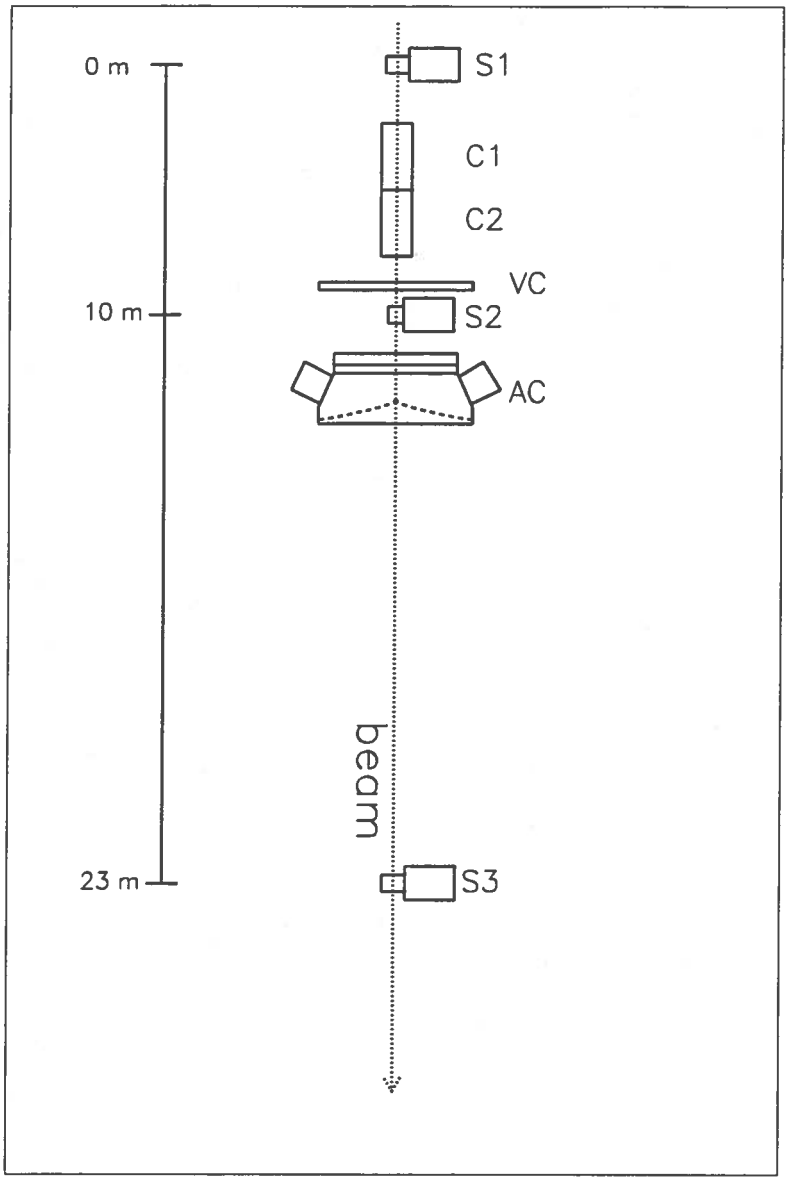

Fig. 5. Schematic view of the experimental set–up used at the PS T10 hall of CERN, with 1 to 4 GeV/c multiparticle beam. S1, S2, S3 are the BC408 scintillators used to define the beam; VC is the beam-halo veto counter; AC indicates the TJNAF aerogel counter; C1, C2 are gas threshold Cherenkov counters permanently installed in the T10 experimental area.

entrance point in the area, and S2 closer to AC. Before S2 a veto scintillator paddle with a circular hole, having a diameter of 4 cm, was also included to prevent triggers due to multiple hits from halo particles. S3, with a size of $10 \times 10 \times 1$ cm^3, was placed 13.25 m behind S2, in the furthest accessible location in the T10 area. The time of flight (TOF) between S1 and S3 allowed a separation of protons with respect to positrons and pions nearly up to the maximum momentum setting used. Each of the three fingers was coupled, by means of short light guides, to the PMT Hamamatsu H2431 (S1 and S3), and H1949 (S2) (rise time $\tau = 0.7$ and 1.3 ns, respectively).

Two CO_2 gas Cherenkov counters (C1 and C2), which are part of the beam line equipment of the experimental area T10, were also used, with pressures set to allow a separation of positrons from pions and protons.

The AC was placed between S2 and S3 facing the incoming beam. Three layers of 3 cm thick aerogel pads were used to form a radiator length of 9 cm, corresponding to the efficiency–optimized thickness, following Ref. [4]. The aerogel tiles provided by Airglass and described in the previous *Sect.* 2.2, were used. Since only six PMTs were reached by Cherenkov photons in the tests done, we have labeled only these, from $A1$ to $A6$, as shown in Fig. 2.

Signals generated by the finger counters and by AC were split by passive splitters to provide energy and timing information. Time was obtained for the finger scintillators through the Ortec 584 constant fraction discriminators (CFD), properly set to minimize the time walk effects within the dynamic range of the detected signals. The discriminator thresholds were set low enough (100 mV), but above the noise level of the phototubes. The discriminated signals of the three fingers fed a coincidence module to define the trigger to accept beam correlated events, and to reject uncorrelated background. In the trigger the beam–halo veto counter was also included. The trigger signal also provided the TDC modules with a common start, and the ADC modules with a gate for charge integration. The electronics for signal digitization and information storage was based on a CAMAC LeCroy TFC-FERA system equipped with memory modules, in order to hold the high counting rates per beam burst.

The analysis of the raw data was carried out off-line in order to identify the different types of particles in the beam and to extract the AC response for the different particles. Beam particle identification (PID) was achieved by means of the TOF technique and by the pulse height distribution analysis of the two C1 and C2 Cherenkov counters. An example of the correlated responses for C1 and C2 at $p = 1$ GeV/c and at $p = 2$ GeV/c is illustrated in Fig. 6. In both situations two clusters of events can be recognized with different accuracy: the low–counts ones are pedestal events, corresponding to pions and protons, which are below the threshold for Cherenkov light emission in CO_2. The high–counts ones are off–pedestal events due to the positron component of the beam,

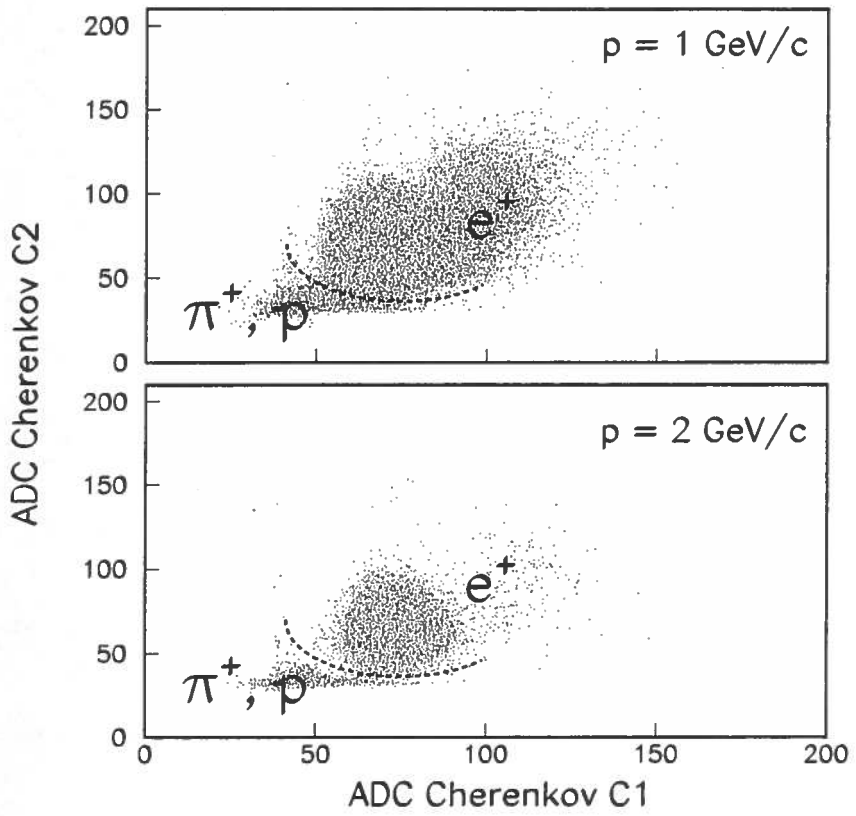

Fig. 6. Correlated response of one of the beam line gas Cherenkov counters versus the other, measured at the least favorable ($p = 1\ GeV/c$) and at a higher ($p = 2\ GeV/c$) momentum setting . Positron events give rise to the off-pedestal distribution, while pions and protons being below the Cherenkov threshold, increment the pedestal counts.

above the Cherenkov threshold. The discrimination of the protons against pions was achieved by the S3–S1 time of flight spectrum, shown in Fig. 7 for the most unfavorable ($p = 4\ GeV/c$) and also at a lower momentum setting ($p = 2\ GeV/c$), with improved separation.

3.2 Data analysis and results

The single PMT efficiency and the overall efficiency of the active channels have been evaluated as the ratio of the off-pedestal ADC counts over the total number of triggers associated to the chosen particle. This procedure implies that a threshold shall be chosen on the ADC counts scale, to discriminate the off-pedestal events from the pedestal ones, which are counted as above or below the Cherenkov threshold, respectively. At a first approach, we have set the threshold at the minimum between the pedestal and the one *p.e.* peak. In the evaluation of the detection efficiency, some events are thus counted as off-pedestal, which are instead related to the physical background due to the production of energetic knock-on electrons (δ-rays) and to the PMT noise and accidental background. While the latter contribution depends only on the PMTs and on the experimental setup, the former is instead particle and momentum dependent, and it is mainly critical for particles below the Cherenkov threshold. This critically affects the rejection properties of the counter.

We have followed also another way of evaluating the detection efficiency, based on the estimation of the total average light yield detected by the active PMTs. When a particle generates Cherenkov light in the radiator, this has to reach the phototube in order to produce a detectable signal. The photons produced undergo scattering and absorption, which affect the final intensity reaching the photocathode. The detection efficiency is thus related directly to the number of *p.e.*s emitted by the photocathode. Namely, if μ is the average number of *p.e.*s, as in Eq. (1), then the efficiency ϵ can be expressed through the equation:

$$\epsilon = 1 - e^{-\mu} \tag{4}$$

where the number of *p.e.*s is assumed to follow a Poisson statistics, thus having a zero *p.e.* emission probability of $e^{-\mu}$. The evaluation of μ for each active PMT is accomplished by fitting the response spectra using Eq. (2), in the same way as for the calibration data. In addition, since the fitting parameters are determined from the calibration procedure, only the parameter μ is searched for in the beam–data analysis.

As an example of the data analyzed, let us consider the nine spectra displayed in Fig. 8. In this figure, the spectra displayed in different columns are obtained by applying the proper cuts onto the time of flight and on the beam–line Cherenkov counters, and refer to positron, pion and proton signal, respectively.

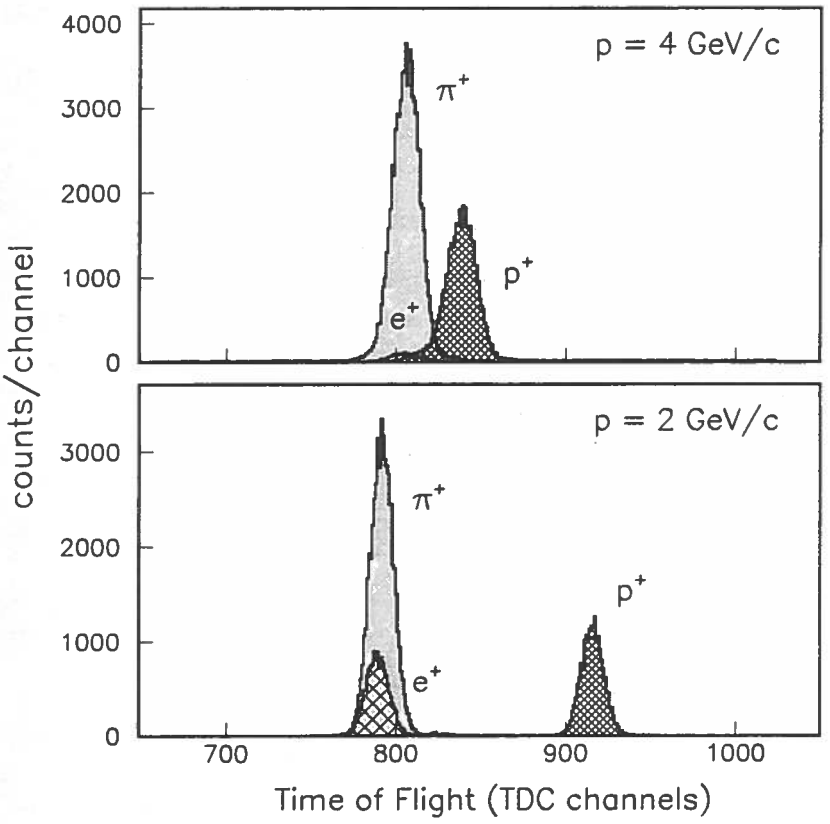

Fig. 7. Spectrum of the S3 time relative to S1 (time of flight) in the least favorable (4 GeV/c) and at a lower (2 GeV/c) momentum setting. The two peaks correspond to protons (rightmost), and to (unresolved) pions and positrons (leftmost). The time spectra are made free from time–walk effects by using constant fraction discriminators. The contributions of pions and positrons to the leftmost peak are separately displayed, as obtained by requiring a coincidence between TOF and C1-C2 counters.

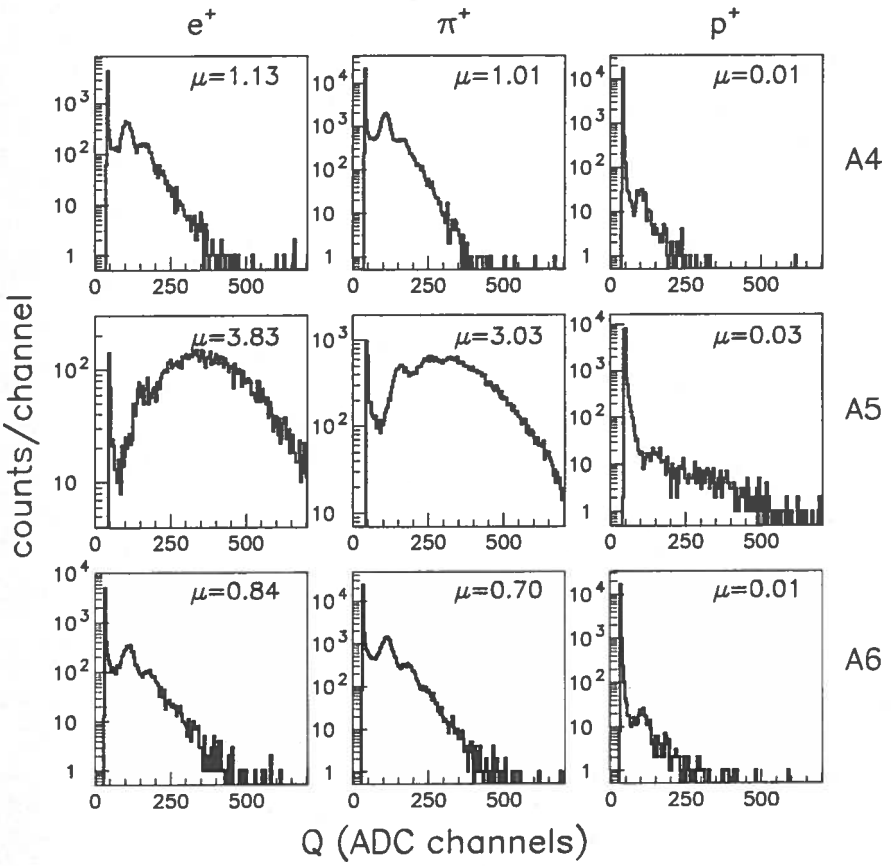

Fig. 8. Measured spectra of the PMTs $A4, A5, A6$ (rows) for a 2 GeV/c beam impinging on the aerogel counter at the location indicated by a cross in Fig. 2. The three columns show the PMTs response for events selected by the PID procedure (e^+, π^+,p , from left to right, respectively). The average number of $p.e.$ μ, estimated by fitting each spectra, is also displayed.

These spectra contain the contributions of three adjacent phototubes on one side of the detector, namely $A4$, $A5$, $A6$, and correspond to the beam impact position defined in *Sect.* 3.1 and displayed in Fig. 2 (cross-mark). It must be noted that the main contribution to the summed response is exhausted by the PMT which is closer to the hit point ($A5$), while the adjacent PMTs contribute to a lesser extent, thus indicating that the directionality of the Cherenkov light produced ($\theta_C = 12.7^o$) is not greatly spoiled by Rayleigh scattering in the aerogel used, which is the most important way the Cherenkov photons get lost. For pions, as an example, the PMT $A5$ detects 64% of the total average light yield detected by the three phototubes $A4, A5, A6$. Moreover, we observe that most of the light produced in this hit position, is collected by the PMTs $A4, A5, A6$. In fact, considering the response to positrons, the total number of *p.e.*s detected by $A4, A5, A6$ equals 5.80, whereas the total contribution of the lower PMTs $A1, A2, A3$ amounts to only 0.73 *p.e.*.

The total number of *p.e.*s is estimated by means of a summation of the contribution of each photomultiplier. This summation can be performed either through an analysis of the analog sum of the individual PMT responses, or through a coherent sum of the number of *p.e.*s detected by the individual PMTs. For example, if we restrict ourselves to the only PMTs $A4, A5, A6$, then following the first method, we construct the sum-spectrum $A4+A5+A6$ starting from the signals of the PMT $A4, A5, A6$, then analyze the resulting distribution by using the fitting procedure previously described in Sec. 2.3, which determines the total average number of *p.e.*s μ. In Fig. 9, we show an example of such an analysis of the different particle summed responses at $p = 2\ GeV/c$. In the second approach, we analyze the individual responses $A4, A5, A6$, as those represented in Fig. 8, getting the average number of *p.e.*s detected by each PMT (μ_4, μ_5, μ_6), then evaluating the total detected, by the sum $\mu = \mu_4 + \mu_5 + \mu_6$.

A comparison between the two methods is performed in Tab. 2, where we list the number of *p.e.*s estimated for the individual PMTs, and the corresponding sum (5.80 *p.e.* for e^+), which is consistent with results from the summed response analysis (5.76 *p.e.* for e^+). In Tab. 2, the values of efficiency are also displayed, as evaluated (ϵ) by means of Eq. (4) from the mean number of *p.e.*s μ, and compared to the efficiency (ϵ') evaluated by the ratio between the off-pedestal to pedestal events counted (at a proper threshold setting). The efficiencies (ϵ'') calculated from the analog sum are also shown to be consistent with the previous results. The inclusion of the other 23 PMTs in the evaluation of μ slightly changes the total detected *p.e.*s (6.8 *p.e.* for e^+, 5.9 *p.e.* for π^+ and 0.07 *p.e.* for p), and does not practically affect the efficiency values.

The efficiency variation with the beam hit point has been also sampled. This check, performed on the three points indicated with dots in Fig. 2, has resulted in an overall efficiency fluctuation of 0.1% at most. Same results have been

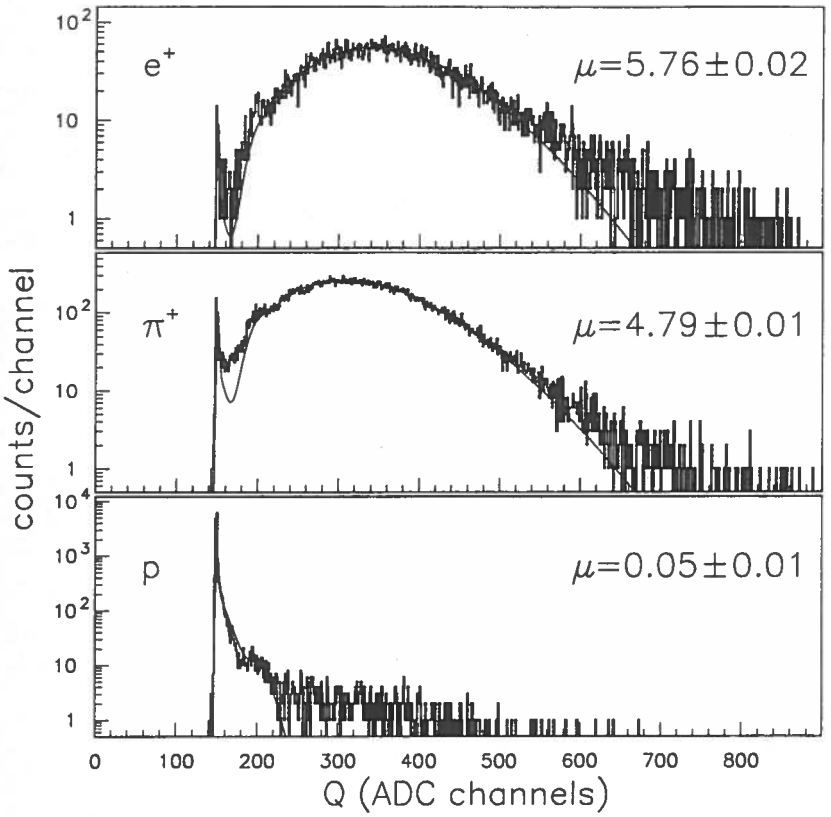

Fig. 9. Spectra of the analog sum of PMTs $A4, A5, A6$ responses at $p = 2\ GeV/c$, gated on different particles of the beam (e^+, π^+, p, from top to bottom, respectively). The curves are obtained by fitting Eq. (2) to the data. The value of the average number of *p.e.* μ deduced from each fit is displayed in either case.

Table 2
The number of *p.e.* detected at a momentum setting $p = 2\ GeV/c$, as evaluated through the fitting procedure displayed in the dedicated figures. ϵ is derived from $\mu = \mu_4 + \mu_5 + \mu_6$; ϵ' is the ratio between off-pedestal to total counts; ϵ'' is derived from the analog sum.

PMT		e^+	π^+	p	Ref.
$A4$	μ_4	1.13	1.01	0.01	Fig. 8
$A5$	μ_5	3.83	3.03	0.03	Fig. 8
$A6$	μ_6	0.84	0.70	0.01	Fig. 8
	$\mu = \mu_4 + \mu_5 + \mu_6$	5.80	4.74	0.05	
	μ *from analog sum*	5.76	4.79	0.05	Fig. 9
	ϵ	0.997	0.991	0.046	
	ϵ'	0.996	0.990	0.104	
	ϵ''	0.997	0.992	0.049	

obtained moving to symmetric points in the lower part of the detector. These results are fully consistent with those of Ref. [4].

The influence of the ADC threshold setting for particles above the Cherenkov threshold and the rejection of those below, has been investigated for the four momentum settings ($p = 1, 2, 3, 4\ GeV/c$), and is visualized in Fig. 10. Here, the e^+ and π^+ detection efficiencies (empty squares and full squares, respectively) are plotted as a function of the threshold, while the proton data are conveniently represented as the detection inefficiency, defined as $1-\epsilon$. Efficiencies are here calculated as the ratio between the off–pedestal to total events detected, at a given threshold. The crossing point of the proton inefficiency with the other efficiency curves, defines an optimal choice of the threshold to maximize the efficiency for pions and minimize the false triggers correlated to proton signals. In Fig. 11 and in Tab. 3 we report the momentum-dependence of the efficiencies for the three types of particles analyzed for a minimum threshold setting, as well as for a threshold chosen according to the criterion based on Fig. 10. In the whole range of momenta $1 - 4\ GeV/c$, at minimum threshold, the efficiency is 99.6% for e^+, 98.6% for π^+, and 12% for p, on average. At an optimized threshold, these reduce to 95.9% for π^+, and about 12% for p on average, thus yielding to a rejection ratio p/π of 5×10^{-2}, estimated as the ratio between the two corresponding efficiencies.

These results, which for electrons agree with the previous results reported in Refs. [3,4], need a discussion as far as the proton triggers are concerned. These are mainly due to two effects: the accidental coincidences of the intrinsic PMT noise together with any other accidental noise sources of the experiment, and the generation of δ-rays, which will yield unwanted Cherenkov events. Light from δ-rays happens primarily for pions, but in this case the efficiencies are not affected, since pions are above the Cherenkov threshold. We have calculated the contribution to the efficiency of p due to δ-rays starting from the microscopic cross-sections [11], and considering all the material layers which the counter is composed of, from the entrance window up to the mirror. The results of such a calculation are summarized in Tab. 4. In this table, it is shown that the main contribution to the δ-rays yield per proton is provided by the aerogel itself. The total estimated yield accounts for nearly up to 3.5% of the misidentified pion triggers due in fact to protons, in the momentum range explored.

In order to evaluate the contribution of the sources of background other than δ-rays, we have performed a measurement with no aerogel pads in the counter, and with air as radiator. Only positrons are above the threshold, with this setup. Moreover, the δ-rays yield for protons in air is estimated to be of the order of 10^{-7} at most in the $1 - 4\ GeV/c$ range. Therefore the events counted above the chosen threshold can be attributed to the other sources of background. These have been measured to amount to 1.5%, regardless of the mo-

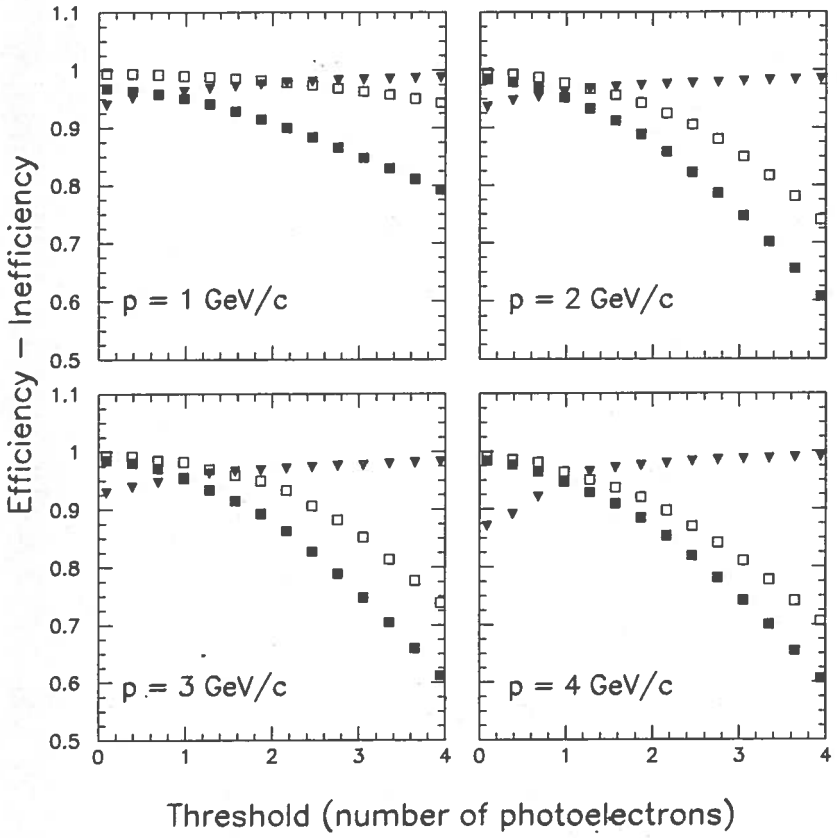

Fig. 10. Efficiency-inefficiency as a function of threshold for the four momenta measured, evaluated as the ratio of the off-pedestal to total number of events. In the plots, empty squares are for positrons, full squares are for pions, while the inefficiency for proton detection is represented as downward full triangles.

Table 3
Comparison of the efficiency at minimum ϵ_π and at optimized $\epsilon_\pi{}'$ threshold, evaluated as the ratio between off–pedestal to total triggers. The average number of *p.e.* μ is derived from ϵ_π by inverting Eq.(4). The p/π best rejection ratio $R_{p/\pi}$ obtained is also listed.

p (GeV/c)	ϵ_π	μ	$\epsilon_\pi{}'$	ϵ_p	$\epsilon_p{}'$	$R_{p/\pi}$
1.0	0.968	3.4	0.951	0.077	0.041	0.043
2.0	0.990	4.6	0.967	0.104	0.043	0.044
3.0	0.989	4.5	0.968	0.096	0.048	0.050
4.0	0.988	4.4	0.947	0.155	0.057	0.060

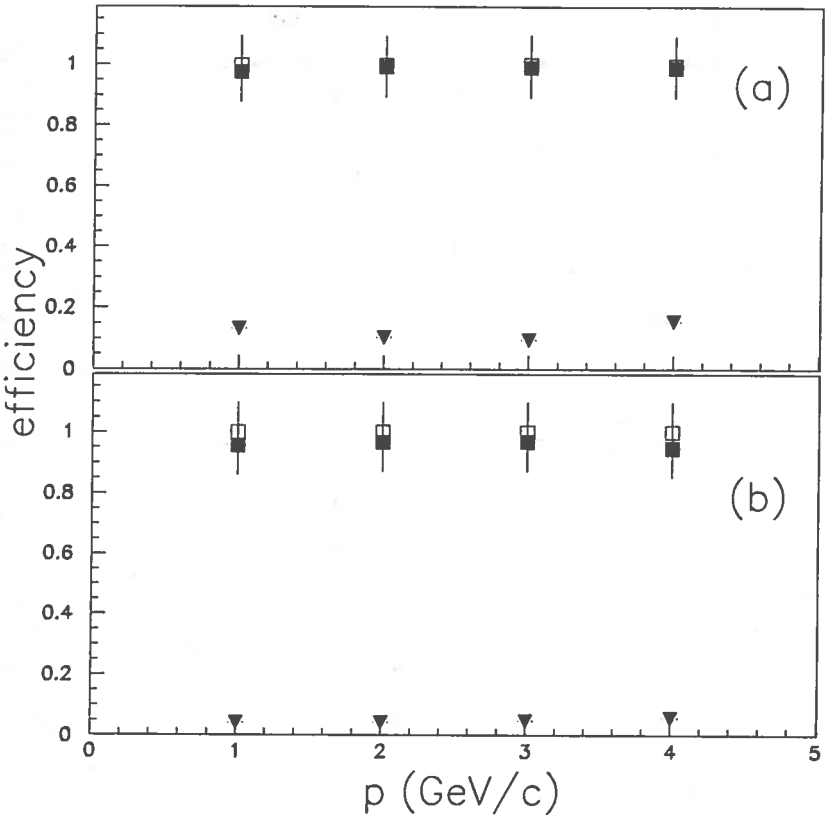

Fig. 11. Efficiency as a function of momentum at minimum (a) and optimized (b) threshold settings. Empty squares are for positrons, full squares for pions, downward full triangles are for protons.

Table 4
Calculated δ-rays production yield per proton expected in the aerogel counter. Contributions from upstream material layers are also considered.

p (GeV/c)	*tedlar*	*carbon fiber*	$Al - Mylar$	*aerogel*	*air*	*total yield*
1.0	–	–	–	–	–	–
2.0	6.4×10^{-5}	2.0×10^{-4}	3.1×10^{-4}	1.7×10^{-2}	–	1.8×10^{-2}
3.0	1.0×10^{-4}	3.2×10^{-4}	5.0×10^{-4}	2.7×10^{-2}	–	2.8×10^{-2}
4.0	1.2×10^{-4}	3.9×10^{-4}	5.9×10^{-4}	3.3×10^{-2}	3.6×10^{-7}	3.4×10^{-2}

mentum. This latter value, summed to the contribution of the δ-rays, accounts for a total estimated background of 5% ($\epsilon_p{}'$) quoted in Tab. 3.

4 Conclusions

The response of the silica aerogel threshold Cherenkov detector to be installed at the TJNAF Hall A has been tested with electrons, pions and protons with momenta ranging from 1 to 4 GeV/c.

Detection efficiencies have been measured for particles above and below the Cherenkov threshold. For a minimum threshold setting, i.e. just below the one *p.e.* peak, we have quoted, for a sub–set of three adjacent phototubes, total detection efficiencies $> 99.6\%$ for positrons, and $> 98.5\%$ for pions on average, with slight fluctuations within the explored momentum range. The inclusion of the other 23 PMTs in the evaluation of μ for e^+ slightly increases the total detected *p.e.*s from 5.8 to 6.8 *p.e.* without practically affecting the efficiency values.

Detection efficiencies for protons, which are false pion triggers, have been measured to be nearly 12% at minimum threshold setting, but these decrease to about 5% if the threshold choice is optimized, i.e. such that $\epsilon_\pi = 1 - \epsilon_p$, which keeps however the pion detection efficiency at the reasonable level of 95.9%.

The contribution of the major sources of background have been identified and estimated, namely the production of energetic knock-on electrons and those related to accidental background. These estimates are in agreement with the measured rate of sub-threshold particle misidentification.

References

[1] *Conceptual Design Report - Basic Experimental Equipment* , CEBAF, Newport News, Virginia (April 13, 1990).

[2] M. Iodice, E. Cisbani, S. Colilli, R. Crateri, S. Frullani, F. Garibaldi, F. Giuliani, M. Gricia, M. Lucentini, A. Mostarda, L. Pierangeli, F. Santavenere, G.M. Urciuoli, R. De Leo, L. Lagamba, A. Leone, R. Perrino, S. Kerohas P. Vernin, submitted to *Nucl. Instr. and Meth.* **A** (1997).

[3] L Alexa, G.M. Huber, G.J. Lolos, F. Farzanpay, A. Leone, R. Perrino, F. Garibaldi, M. Iodice, D. Humphrey, Z. Papandreou, P. Ulmer, R. De Leo, *Nucl. Instr. and Meth.* **A 635** (1995) 299.

[4] G.J. Lolos, G.M. Huber, L.C. Alexa, F. Farzanpay, M. Iurescu, Z. Papandreou, A. Weinerman, A. Leone, R. Perrino, F. Garibaldi, M. Iodice, *Nucl. Instr. and Meth.* **A 385** (1997) 403.

[5] *Burle Industries Inc.*, 1000 New Holland Ave., Lancaster, PA 17601, USA.

[6] *Airglass AB*, Box 150, S24500 Staffanstorp, Sweden.

[7] D.E. Fields et al., *Nucl. Instr. and Meth.* **A 34** (1994) 431.

[8] R. De Leo, L. Lagamba, V. Manzari, E. Nappi, T. Scognetti, M. Alemi, H. Becker, R. Forty, I. Adachi, R. Suda, T. Sumiyoshi, A. Leone, R. Perrino, C. Matteuzzi, J. Seguinot, T. Ypsilantis, E. Cisbani, S. Frullani, F. Garibaldi, M. Iodice, G.M. Urciuoli, "Electronic detection of focused Cherenkov rings from aerogel", *Nucl. Instr. and Meth.* **A** (1997) (in print).

[9] Bellamy et al., *Nucl. Instr. and Meth.* **A 339** (1994) 468.

[10] K. Batzner, D. Dumollard, L. Durieu, D.J. Simon, F. Cataneo, and M. Ferro–Luzzi, CERN PS/PA–EP Note 88-26.

[11] GEANT, Detector description and simulation tool, *CERN Program Library* **W5013** (Long write-up).